Fourier information optics for the ultrafast time domain

Andrew M. Weiner

School of Electrical and Computer Engineering, Purdue University, West Lafayette, Indiana 47907-1285, USA

amw@purdue.edu

Received 23 May 2007; revised 6 September 2007; accepted 7 September 2007;
posted 11 September 2007 (Doc. ID 83200); published 26 November 2007

Ultrafast photonic signal processing based on Fourier optics principles offers exciting possibilities to go beyond the processing speeds of electronics technologies for applications in high-speed fiber communications and ultrawideband wireless. I review our recent work on processing of ultrafast optical signals via conversion between time, space, and optical frequency (Fourier) domains. Specific topics include optical arbitrary waveform generation, application of optical pulse shaping technologies for wavelength-parallel compensation of fiber transmission impairments and for experimental studies of optical code-division multiple-access communications, and application of photonic methods for precompensation of dispersion effects in wireless transmission of radio-frequency signals over ultrawideband antenna links.

OCIS codes: 320.5540, 060.7140, 320.5520.

1. Introduction

Emmett Leith, in whose memory this journal feature issue is dedicated, was a pioneer of the fields of information optics, holography, optical signal processing, and imaging [1–4]. Much of his work drew heavily on the natural ability of optics to perform Fourier transforms in the spatial domain, e.g., in holographic recording of an object's Fourier spectrum or in correlation processing via spatial filtering at a Fourier plane. His research was concerned both with applications to information that was inherently optical (e.g., optical imaging) and to information in the microwave domain that could be processed optically (e.g., synthetic aperture radar). During the latter part of his career, he was also active in research in which Fourier principles in the time and optical frequency domains were exploited for imaging in scattering media via holographic range gating [5].

This paper surveys the author's research on Fourier processing of ultrafast (picosecond and femtosecond) time-domain optical signals. As sketched in Fig. 1, this research exploits mappings and transforms between fields in the spatial, temporal, and optical frequency domains. In particular, this paper focuses on methods for ultrafast optical waveform synthesis and signal processing based on spatial manipulation of the dispersed optical frequency spectra of femtosecond pulses. Using these methods, femtosecond pulses can be engineered into complex optical signals according to specification. A key point is that waveform synthesis is achieved by parallel modulation in the frequency domain, which is achieved by spatial modulation of the spatially dispersed optical frequency spectrum. Thus, waveforms with effective serial modulation bandwidths as high as terahertz can be generated and manipulated without requiring any ultrafast modulators.

As applications of such optical processing methods, we discuss compensation of fiber transmission impairments, including both chromatic dispersion and polarization-mode dispersion, as well as novel optical communication systems based on encoding and decoding of ultrafast pulses. These examples exploit time–frequency Fourier techniques to perform matched filtering processing of ultrafast pulsed signals, in close analogy with the spatial Fourier techniques used by Leith and his colleagues for correlation processing of spatial domain optical signals. We also discuss experiments in which we have applied time-domain Fourier pulse processing technology for generation of arbitrarily-shaped radio-frequency (RF) electrical waveforms and compensation of chromatic dispersion in wireless transmission of ultrawideband RF signals over broadband antenna links. Again, this use of time-

0003-6935/08/0400A88-9$15.00/0

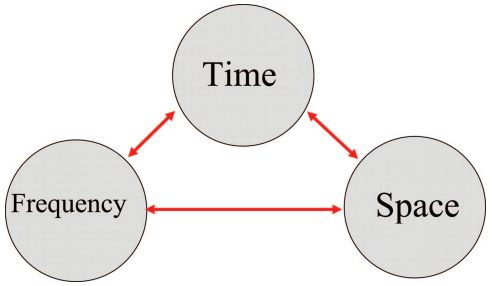

Fig. 1. (Color online) Parallel processing of ultrafast time-domain optical signals is accomplished via frequency-domain manipulation, which is implemented by hardware mapping of optical frequency onto a spatial axis.

domain optical processing for manipulation of RF electrical signals may be seen as broadly analogous to the much earlier use of spatial-domain optical processing for manipulation of microwave (radar) signals.

2. Optical Pulse Shaping

We first discuss femtosecond pulse shaping, in which powerful Fourier synthesis methods are utilized to generate almost arbitrarily shaped femtosecond optical waveforms [6,7]. As sketched in Fig. 2(a), in pulse shaping an incident femtosecond pulse is spread into its constituent spectral components by a grating and lens. A spatially patterned mask then modulates the phase and amplitude of the spatially dispersed spectral components. After the spectral components are recombined by a second lens and grating, a shaped output pulse is obtained, with the pulse shape given by the Fourier transform of the pattern transferred by the mask onto the spectrum. Examples of shaped pulses are shown in Figs. 2(b) and 2(c). Pulse shaping masks were originally implemented by using microlithographic patterning techniques and subsequently by using programmable spatial light modulators, acousto-optic modulators [8], holographic masks, and deformable mirrors. In our laboratory, pulse shaping is normally performed using programmable liquid crystal modulator arrays [9,10] that allow independent, simultaneous gray-level control of both spectral amplitude and phase. Pulse shaping is now used in laboratories around the world for a broad range of applications, including coherent control over ultrafast physical processes, high field physics, nonlinear optical biomedical imaging, and high-speed communications. A review of some of these applications is given in Refs. [7,11].

In our work and in the examples described below, we generally emphasize manipulation of spectral phase, which, compared to other spectral parameters, arguably has the most fundamental impact on temporal waveforms. We note, however, that spectral amplitude filtering, using optical arrangements based on that of Fig. 2, is commonly employed in wavelength-division multiplexed (WDM) optical communications for subsystems such as spectral gain equalizers and reconfigurable optical add–drop multiplexers [12]. Furthermore, polarization pulse shaping, in which the spectral or temporal polarization profile of a pulse is manipulated, has become a topic of significant current interest [13]. Polarization pulse shaping has applications both in fundamental areas such as attosecond pulse generation and coherent control and in technology, such as our work on compensation of polarization mode dispersion (PMD) (discussed later in this paper).

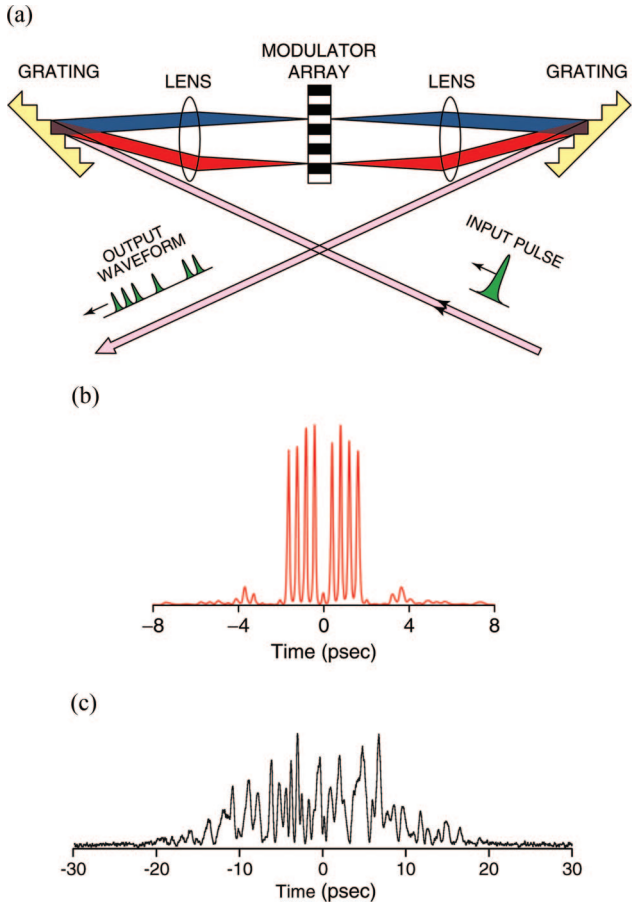

Fig. 2. (Color online) (a) Femtosecond pulse-shaping apparatus and examples of shaped pulses: (b) an ultrafast optical data packet with effective modulation rate of 2.5 THz, and (c) a deterministic femtosecond pseudonoise burst used in studies of optical code-division multiple-access communications.

3. Pulse Processing for Ultrafast Fiber Optics

Pulse shaping technology provides the possibility not only to synthesize ultrafast optical waveforms according to user specification, but also to process such signals. In particular, pulse shapers may be programmed to act as matched filters for waveforms with specific spectral phase signatures, resulting in compression of chirped or distorted input signals to the bandwidth limit. In the following, three applications of such matched filtering relevant to ultrafast fiber communications are described.

A. Chromatic Dispersion Compensation

An interesting first example centers on compensation of chromatic dispersion, which broadens the dura-

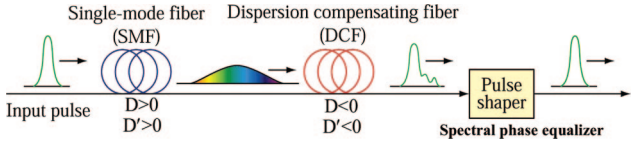

Fig. 3. (Color online) Block diagram of femtosecond dispersion compensation experiments in which a pulse shaper functions as a spectral phase equalizer.

tions of ultrashort pulses sent through fiber optic links. Unless compensated, such broadening leads to intersymbol interference that limits the bit rates of high-speed optical fiber communication links. Physically, chromatic dispersion represents a frequency-dependent (or wavelength-dependent) group velocity. Such group velocity dispersion can also be expressed in terms of the frequency-dependent delay $\tau(\omega)$ and frequency-dependent phase $\psi(\omega)$, which are related through the relation

$$\tau(\omega) = -\frac{\partial \psi}{\partial \omega}. \quad (1)$$

Hence, if a pulse experiences chromatic dispersion $\tau(\omega)$, one can compensate for the resulting broadening by programming a pulse shaper to impose a spectral phase function equal and opposite to that specified in Eq. (1).

A block diagram of experiments demonstrating such dispersion compensation is shown in Fig. 3. Here a programmable pulse shaper was used to complement fiber dispersion compensation techniques in propagating sub-500 fs pulses over optical fiber links ranging from 3 km in early experiments to 50 km most recently [14–16]. In all cases the link consisted of a length of standard single-mode fiber (SMF) concatenated to an approximately matching length of dispersion compensating fiber (DCF). Since SMF and DCF have dispersion with opposite signs at the operating wavelength, the fiber lengths can be adjusted to cancel all of the lowest order dispersion (i.e., phase varying quadratically with frequency). In addition, since the derivatives of the dispersion with respect to frequency also have opposite signs, the dispersion slope (i.e., cubic spectral phase variations) can be partially compensated. In the experiments in Ref. [16], ~460 fs input pulses at 1542 nm center wavelength are first broadened ten thousand times to ~5 ns in propagating through the SMF, then recompressed by the DCF to within a factor of 2 of the input pulse duration. Intensity cross-correlation measurements of the input pulse and output pulse after 50 km fiber propagation are shown in Figs. 4(a) and 4(b), respectively. The remaining broadening and distortion of the output pulse are characteristic of cubic spectral phase variation. At this point the pulse shaper is used to apply a spectral phase function that is equal and opposite to the estimated residual phase variation. Both the actual applied phase function, which is a cubic function modulo 2π [Fig. 4(e)], as well

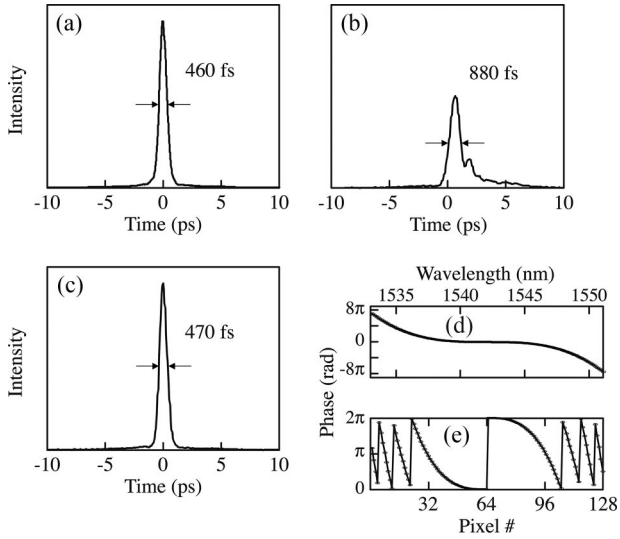

Fig. 4. Distortionless transmission over 50 km fiber via spectral phase equalization. Intensity correlation measurements of (a) input pulse, (b) distorted pulse after propagation through 50 km fiber and partial compensation by dispersion compensating fiber, and (c) restored pulse after spectral phase equalization in a pulse shaper. (d) Unwrapped and (e) actual spectral phase profile programmed onto the liquid crystal modulator.

as the unwrapped version showing a continuous cubic phase [Fig. 4(d)], are plotted for purposes of illustration. Application of the inverse spectral phase function results in a completely recompressed pulse with essentially the original pulse duration (~470 fs) and no observable distortion [Fig. 4(c)]. Thus, in these experiments all-fiber techniques are used for coarse dispersion compensation, while a programmable pulse shaper is used as a spectral phase equalizer to fine tune away any remaining dispersion. In a completely analogous fashion, programmable pulse shapers are now used extensively in compensation of residual dispersion in chirped pulse amplifier systems and in few-cycle pulse generation.

B. Polarization-Mode Dispersion Compensation

We have also performed a series of experiments in which a pulse shaper is used to compensate for polarization-mode dispersion (PMD) in optical fiber. PMD arises from small and essentially random birefringences in single-mode optical fiber [17,18]. Some of the basics of PMD may be understood on the basis of a random wave plate model, illustrated in Fig. 5. Here each wave plate is assumed to have a differential delay $\Delta\tau$ between its birefringent axes, and different wave plates are assumed to have random rotation angles. The delay experienced by an input signal depends on the input polarization and experiences essentially a random walk process. The mean differential group delay observed at the output scales as $\Delta\tau\sqrt{N}$, where N is the number of wave plates. This corresponds to the finding that in real fibers, the mean differential group delay contributed by PMD scales as the square root of fiber length. PMD-induced impairments of optical fiber transmission

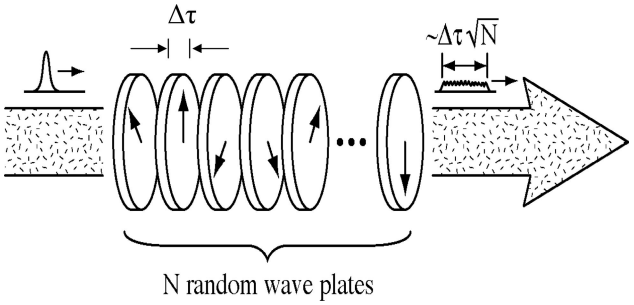

Fig. 5. Random wave-plate picture of polarization-mode dispersion. Each wave plate is assumed to have a differential delay $\Delta\tau$ between birefringent axes.

systems at 10 Gbit/s data rates and (especially) higher, as well as possible compensation of such impairments, is the subject of intense research interest.

We have been interested in compensation of PMD for subpicosecond pulses with large PMD (distortions significantly greater than the pulse duration). When PMD is large, it produces complex pulse distortions involving a frequency-dependent scrambling of the optical polarization state as well as frequency- and polarization-dependent delays. For small PMD (distortions small compared to the pulse duration), PMD is usually treated in a Taylor series expansion framework in optical frequency and characterized as first-order PMD, second-order PMD, etc. Most work on PMD compensators has focused on the first-order PMD regime. However, for large delay distortions bands and sufficiently broad optical bandwidths, the Taylor series expansion breaks down, and an all-order PMD description, in which the signal experiences arbitrary frequency-dependent delay and polarization distortions, is necessary. In our work we adopt this all-order view and aim to sense and correct polarization state and spectral phase in parallel on a wavelength by wavelength basis. Our experiments, to our knowledge, are the first to demonstrate full compensation of PMD in the "all-order" regime [19,20].

Experimental results are illustrated in Fig. 6. Here clean input pulses, with ~600 fs duration and spectral content from 1542 nm to 1556 nm, are coupled into a home-made PMD emulator with 1.5 ps mean differential group delay. The upper plots show Poincare sphere representations of the frequency-dependent state of polarization (SOP). The input pulse prior to the emulator has a frequency-independent SOP, corresponding to a single point on the Poincare sphere (not shown). After the emulator, the SOP exhibits a complex, frequency-dependent trajectory on the Poincare sphere, which is characteristic of PMD in the all-order regime. The frequency-dependent state of polarization is measured using a home-built wavelength-parallel polarimeter [21] and then corrected using a pulse shaper setup, configured such that arbitrary input polarization may be transformed to a fixed linear state (independently and in parallel for each optical frequency component). As a result, the corrected SOP spectrum is restored to approximately a single point on the Poincare sphere. The insertion loss of the state-of-polarization pulse shaper is approximately 7.6 dB. Now we examine the pulse distortion in the time domain, shown in the middle and lower rows of Fig. 6. The clean sub-600 fs input pulses are significantly distorted and spread to several picoseconds as a result of the PMD. Note that the intensity profile of the distorted pulse is actually the sum of the intensities measured separately on two orthogonal polarization basis states. After SOP correction, the pulse is not yet compensated and in fact exhibits further broadening. This is expected as the spectral phase is not yet corrected, and the polarization correction operation in the pulse shaper adds additional spectral phase. However, the SOP correction transforms the complicated vector pulse distortion problem into a scalar generalized dispersion compensation problem. Using a second pulse shaper to compensate the spectral phase (4.5 dB insertion loss), as in Subsection 3.A, restores a clean input pulse, with duration similar to that of the input pulse.

Our overall PMD compensation experiment may be viewed as a vector and ultrafast time-domain generalization of the Fourier-optic matched filtering and correlation processing techniques known since the 1960s for processing of spatial domain optical signals.

C. Ultrashort Pulse Optical Code-Division Multiple Access

In a third example, we apply pulse shapers for experimental studies of optical code-division multiple-access (O-CDMA) lightwave communications. CDMA derives from radio frequency (RF) spread spectrum communications [22], originally developed for military applications due to an inherent low probability of intercept and immunity to interference, and more recently a key technology for commercial RF cellular radio applications. Although still exploratory, research aimed at extending CDMA to the optical domain (O-CDMA) is a topic of strong current interest. In O-CDMA, different users whose signals may be overlapped both in time and frequency share a common communications medium; multiple access is achieved by assigning different, minimally interfering code sequences to different CDMA transmitters, which must subsequently be detected in the presence of multiaccess interference from other users. Compared to mainstream optical communications approaches, such as time-division multiplexing and wavelength-division multiplexing, O-CDMA is of interest due to intriguing possibilities for simplified and decentralized network control, potential improved spectral efficiency, soft-limited capacity, physical layer security, and increased flexibility in the granularity of bandwidth that can be provisioned [23].

Since RF-CDMA works with typical carrier frequencies in the ~1 GHz range and bit rates of the order of ~100 kbits/s, current electronic technologies can easily provide coding techniques and long temporal codes (~1000 chips) for each bit, which is critical to support a large number of potential users. In

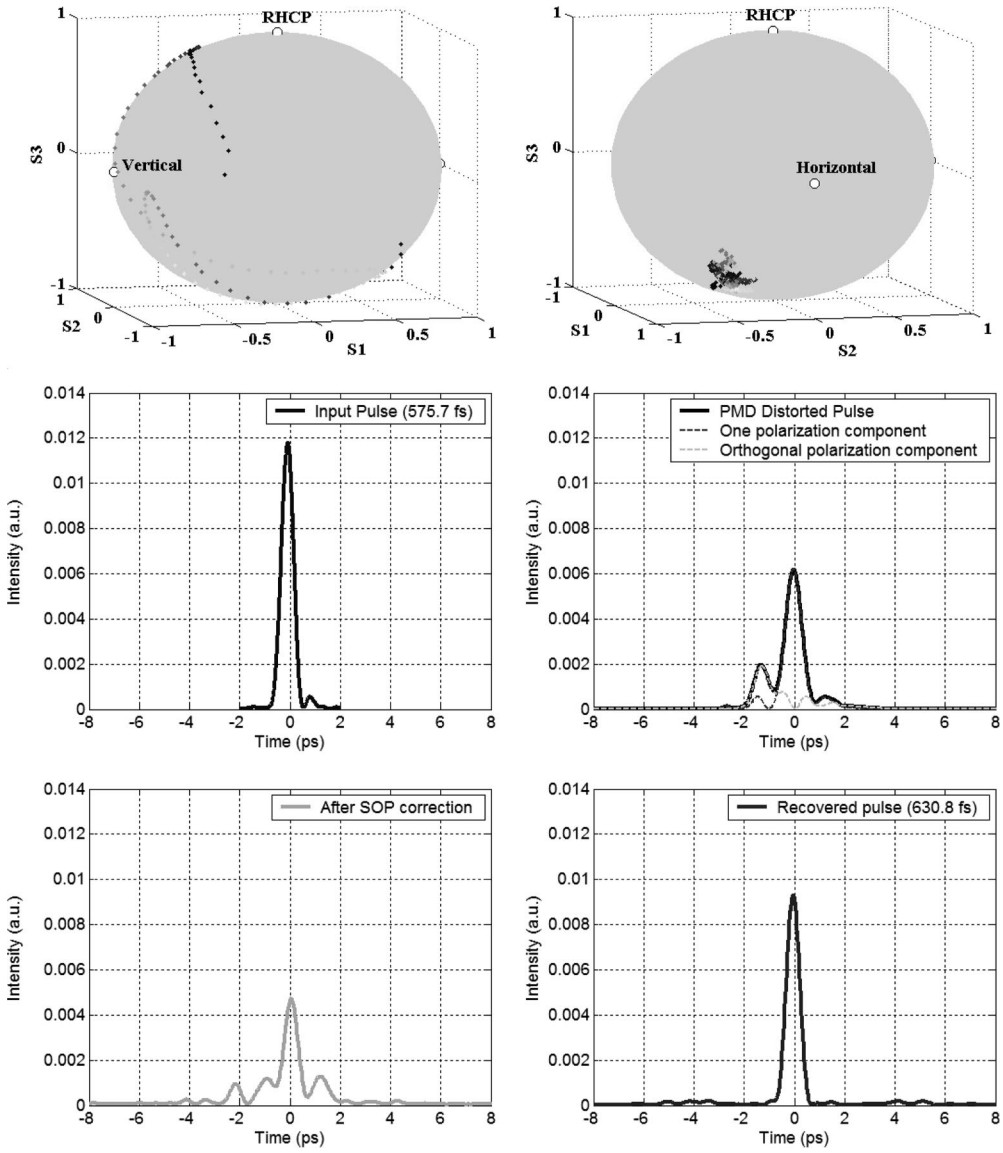

Fig. 6. Data on all-order PMD compensation. The top row displays SOP versus wavelength before and after PMD compensation. The middle and the bottom rows show the time-domain waveforms at the input, and after each PMD compensation step.

addition, the system bit error rate requirement is usually not so strict for RF-CDMA. In contrast, the need to perform encoding and decoding for O-CDMA poses one immediate challenge both because of the optical carrier frequency and the much higher bit rates (multiple Gbits/s per user), which already approaches the limit of electronic processing. Therefore, innovative all-optical processing technologies are needed.

One of the earliest approaches to achieve encoding and decoding at the high rates needed for optical communications is spectral phase encoding, first analyzed in Ref. [24]. Here a pulse shaper is used to impart a spectral phase code onto the optical spectrum. For the case of a pseudorandom phase code, this transforms a bandwidth-limited input pulse into a pseudonoise burst in time, such as shown in Fig. 2(c). At the receiver a second pulse shaper can be programmed with a conjugate phase code, such that incoming signals with the matching code are recompressed (decoded) into short pulses. Multiaccess interference from other users with different codes is not correctly decoded and hence remains in the form of low intensity pseudonoise signals. The desired (matching) signal can then be picked out on the basis of its higher peak intensity.

References [25,26] provide recent reviews of O-CMDA, with an emphasis on experimental progress in spectral phase encoded approaches. Figure 7 shows the schematic experimental setup for four-user O-CDMA data transmission experiments at 2.5 Gbits/s and 10 Gbits/s per user performed in the author's laboratory at Purdue University [27,28]. An actively mode-locked fiber laser followed by a dispersion decreasing fiber soliton compressor producing nearly transform-limited ~0.4 ps pulses at 10 GHz

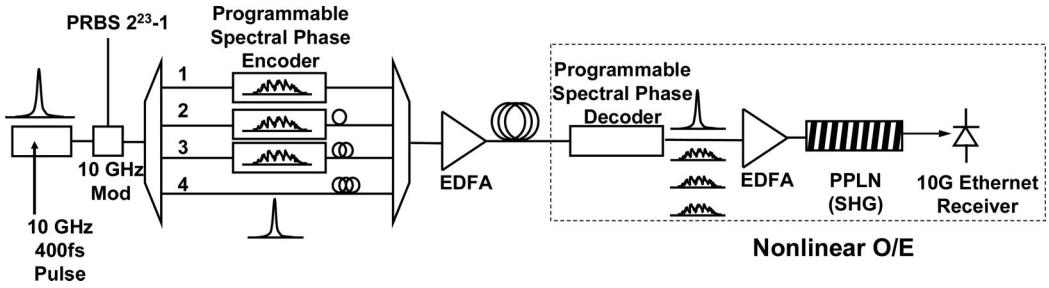

Fig. 7. Experimental system for four-user O-CDMA system experiments.

repetition rate centered near 1542 nm is used as the pulse source. Pseudorandom data at either 2.5 Gbits/s or 10 Gbits/s is impressed onto the pulse using an integrated intensity modulator for on–off keying. For three users, the modulated ultrashort pulses are input into programmable fiber-coupled pulse shapers for spectral phase encoding. A fourth uncoded user path is also present as an additional interference channel. The receiver also contains a programmable fiber-coupled pulse shaper, which is used to select (decode) the desired user channel. Figure 8 demonstrates the ability to properly decode any of the four user channels by the correct selection of decoder spectral phase code; here, a length-31 maximal-length-sequence code. The figure shows intensity cross correlation measurements measured directly after the decoder. Clearly in each case a strong intensity contrast is obtained for the selected code waveform, relative to the unmatched multiaccess inteference. It is interesting to point out that a particular improperly decoded user has different waveform structures when different channels are selected for decoding, as shown in the insets.

Note that in this experiment, the pulses from each user are roughly separated by ~25 ps in a time-slotted O-CDMA scheme; there is no need for precise control of the time offsets. In general, O-CDMA experiments have ranged from fully synchronous (which allows best suppression of multiaccess interference and hence highest performance, at the cost of increased complexity in implementation and network management) to fully asynchronous (simplest in terms of implementation, but with reduced performance). The time-slotted example described here represents a compromise providing intermediate performance and implementation complexity. For a fuller discussion of such issues, see Refs. [25,26].

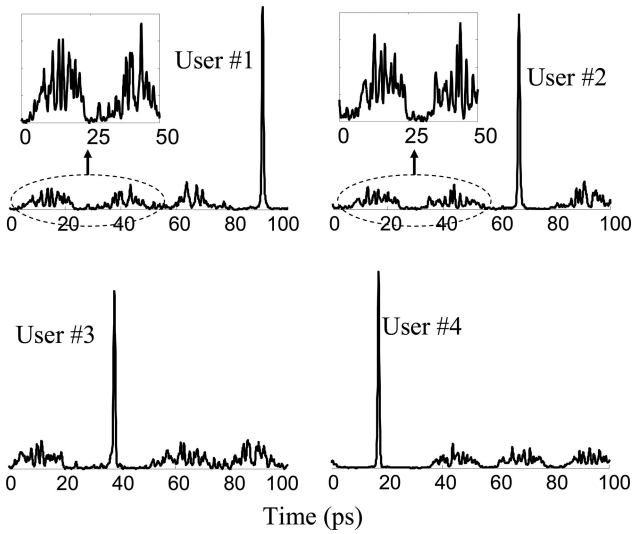

Fig. 8. Intensity cross-correlation measurements of properly decoded channels 1 to 4 demonstrating the ability to selectively decode any of four user channels in spectral phase encoding O-CDMA experiments.

Following the decoding stage, a nonlinear intensity discriminator or other nonlinearity is needed to distinguish between properly and improperly decoded users. This is because the intensity differences seen in Fig. 8 occur on a time scale too fast to directly distinguish using electronics. In our work we implement this nonlinear discrimination function using an optical amplifier and a highly sensitive fiber-pigtailed periodically-poled lithium niobate waveguide device that performs second harmonic generation. At the output of the nonlinear discriminator, the error-free data from the selected channel is successfully recovered using a 10 Gbit/s Ethernet photoreceiver. Details may be found in Refs. [27,28].

4. Photonic Processing for Ultrawideband Wireless

In the previous section we showed examples of photonic processing for manipulation of ultrashort pulses too fast for direct manipulation via conventional electronic or optoelectronic means. In this section we discuss the application of photonic processing for generation and manipulation of ultrawideband, pulsed electrical signals, again in a domain where conventional electronic solutions do not yet exist.

Optical pulse shaping can be applied to realize arbitrary waveform generation capability for ultrawideband radio-frequency (RF) electrical signals. Exploiting the well developed optical pulse shaping technology, an ultrashort optical input pulse is first shaped as desired, then directed to a fast optical-to-electrical converter (O/E). By controlling the optical excitation waveform onto the O/E, programmable cycle-by-cycle synthesis of burst RF waveforms can be achieved. This results in a unique technology for generation of waveforms with instantaneous bandwidths far beyond the reach of commercial electronic arbitrary waveform generator solutions, whose band-

widths are limited to 1–2 GHz. Different choices of pulse shaper configurations, coupled with different choices of O/E converter technologies, has allowed demonstrations of waveform generation from the GHz to the THz. Hence this approach is scalable over several orders of magnitude in RF frequency. Reviews are presented in Refs. [29,30].

As an example, here we focus our attention on generation of subnanosecond RF waveform bursts in the 3.1 to 10.6 GHz band allocated by the Federal Communications Commission (FCC) for ultrawideband (UWB) wireless communications. Because traditional grating based optical pulse shapers are generally limited to generation of waveforms confined to time apertures of the order of 100 ps, we adopt a modified generator approach, sketched in Fig. 9(a) [31,32]. Here we rely on the ability to sculpt the optical power spectrum of a short optical pulse using a pulse shaper, followed by optical frequency-to-time conversion in a dispersive medium. Typically in our experiments, we use ~100 fs input pulses from a mode-locked fiber laser, a reflective-geometry pulse shaper for modulating the power spectrum, and ~5.5 km of single-mode fiber for dispersion. The fiber is sufficiently long that its chromatic dispersion provides a unique mapping from optical wavelength to temporal position in the output optical intensity waveform (voltage waveform after O/E conversion). Figures 9(b) and 9(c) show an example of a shaped optical power spectrum and the resultant electrical burst that is frequency hopped from 1.2 GHz to 2.5 GHz to 4.9 GHz [32]. As the data clearly demonstrate, the generated time-domain RF waveform is a directly scaled version of the tailored optical power spectrum. The RF waveform described here, composed of abrupt frequency hops over a several GHz band on a cycle-by-cycle basis, cannot be generated with any existing electronic technology.

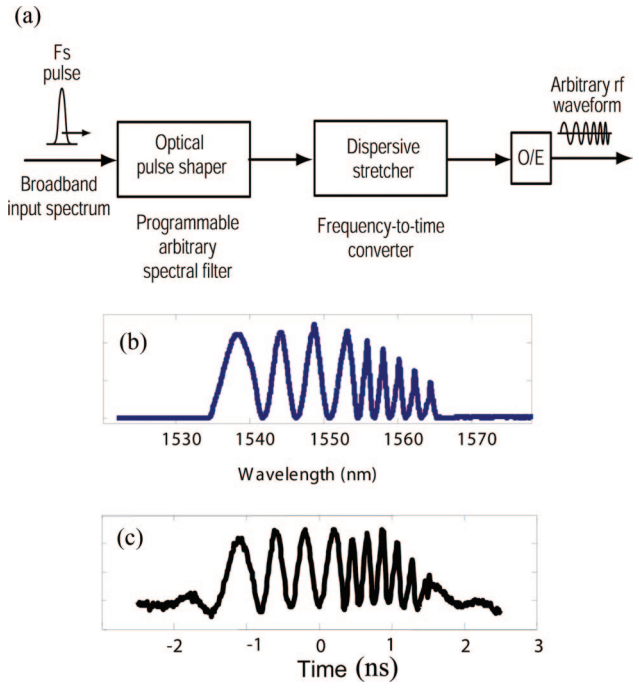

Fig. 9. (Color online) (a) Photonic RF-AWG concept employing frequency-to-time conversion. (b) Shaped optical power spectrum, and (c) resultant RF burst showing 1.2–2.5–4.9 GHz frequency hoping on a cycle-by-cycle basis.

Such electrical waveform shaping enables a number of new experimental possibilities. As one example, we discuss the use of such electrical waveform shaping to allow compensation of dispersive effects due to the antennas used in UWB wireless links. This work is completely analogous to the optical dispersion compensation experiments of Subsection 3.A and constitutes the first hardware implementation of dispersion compensation in the UWB electrical domain [33].

Antenna dispersion, associated with a frequency-dependent phase response and hence frequency-dependent delay, is an important issue in UWB, as many common antennas that have been optimized for broadband amplitude response do not exhibit linear spectral phase (this is especially true for directional broadband antennas). The concept of optimizing the antenna feed voltage to obtain desirable temporal properties in the received waveforms, such as peak amplitude or minimal duration, has been explored theoretically [34], but could not previously be tested experimentally due to lack of waveform generation capability. Using our photonic generator technology, we have recently published the first such experiments (setup sketched in Fig. 10), using a pair of 1–12 GHz TEM horn antennas [33]. In these experiments simple (unshaped) voltage drive pulses led to strongly chirped waveforms spread over a time aperture of many nanoseconds after the receive antenna. In contrast, by using an appropriately preshaped drive, we achieved strongly compressed ~80 ps pulses after the receiving antenna. In current work we are working to extend such precompensation experiments to much more compact planar or near-planar antenna structures. Figure 11 shows new unpublished results on the response of a (minimally dispersive) broadband planar bow-tie antenna transmitter and a (strongly dispersive) spiral antenna receiver [35]. Figures 11(a) and 11(b) show a photonically synthesized drive pulse with ~250 ps duration and 4.5 GHz electrical bandwidth around 5 GHz center frequency and the result-

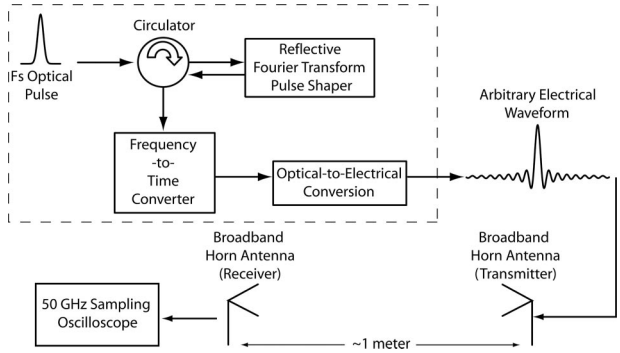

Fig. 10. Schematic setup for experiments in which ultrawideband electrical pulses are intentionally shaped in order to precompensate dispersion from a broadband antenna pair.

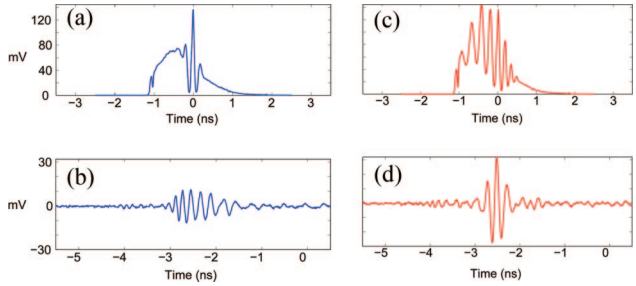

Fig. 11. (Color online) Demonstration of dispersion precompensation for broadband bowtie-spiral antenna pair: (a) impulsive drive waveform; (b) received signal from spiral antenna, showing strong pulse distortion and broadening due to dispersion; (c) shaped precompensation drive waveform; (d) compensated received signal.

ing received waveform with ~1.4 ns duration and strong down-chirp. Figure 11(c) shows an up-chirped precompensation drive waveform designed to have temporal dispersion opposite to the received waveform of Fig. 11(b) while maintaining RF spectral amplitude and bandwidth. The resulting received waveform, Fig. 11(d), is substantially compressed, exhibiting virtually no observable chirp, ~3× reduction in duration (to 490 ps), and ~3× increase in received peak voltage. The ability to precompensate antenna distortions should significantly extend the choices of antenna structures that can be applied to UWB wireless.

5. Conclusion

In summary, I have given a brief introduction to ultrafast optical waveform generation and processing based on parallel manipulation in the optical Fourier domain. In addition to applications to optics, recent progress in extending these technologies to ultrawideband, radio-frequency electrical signals was also discussed. This line of research may be considered as an analog of Fourier processing concepts known in the context of spatial domain optical signals from the 1960s, but now applied to the ultrafast time domain where electronic technologies are not expected to compete in the foreseeable future.

This work was performed in collaboration with numerous students and colleagues at Purdue University, whose contributions are gratefully acknowledged. This work was supported in part by the National Science Foundation under grant 0501366-ECS, the Army Research Office under grant DAAD19-03-1-0275, and DARPA under grant MDA972-03-1-0014.

References

1. E. N. Leith and J. Upatnieks, "Reconstructed wavefronts and communication theory," J. Opt. Soc. Am. **52,** 1123–1130 (1962).
2. L. J. Cutrona, E. N. Leith, C. J. Palermo, and L. J. Porcello, "Optical-data processing and filtering systems," IRE Trans. Inf. Theor. **6,** 386–400 (1960).
3. L. J. Cutrona, E. N. Leith, L. J. Porcello, and W. E. Vivian, "On application of coherent optical processing techniques to synthetic-aperture radar," Proc. IEEE **54,** 1026–1032 (1966).
4. E. N. Leith, "Quasi-holographic techniques in microwave region," Proc. IEEE **59,** 1305–1318 (1971).
5. H. Chen, Y. Chen, D. Dilworth, E. Leith, J. Lopez, and J. Valdmanis, "Two-dimensional imaging through diffusing media using 150-fs gated electronic holography techniques," Opt. Lett. **16,** 487–489 (1991).
6. A. M. Weiner, J. P. Heritage, and E. M. Kirschner, "High-resolution femtosecond pulse shaping," J. Opt. Soc. Am. B **5,** 1563–1572 (1988).
7. A. M. Weiner, "Femtosecond pulse shaping using spatial light modulators," Rev. Sci. Instrum. **71,** 1929–1960 (2000).
8. J. X. Tull, M. A. Dugan, and W. S. Warren, "High resolution ultrafast laser pulse shaping and its application," in Vol. 20 of *Advances in Magnetic and Optical Resonance,* W. S. Warren, ed. (Academic, 1997), pp. 1–66.
9. A. M. Weiner, D. E. Leaird, J. S. Patel, and J. R. Wullert, "Programmable shaping of femtosecond pulses by use of a 128-element liquid-crystal phase modulator," IEEE J. Quantum Electron. **28,** 908–920 (1992).
10. M. M. Wefers and K. A. Nelson, "Generation of high-fidelity programmable ultrafast optical waveforms," Opt. Lett. **20,** 1047–1049 (1995).
11. A. M. Weiner, "Femtosecond optical pulse shaping and processing," Prog. Quantum Electron. **19,** 161–238 (1995).
12. J. E. Ford and J. A. Walker, "Dynamic spectral power equalization using micro-opto-mechanics," IEEE Photon. Technol. Lett. **10,** 1440–1442 (1998).
13. T. Brixner and G. Gerber, "Femtosecond polarization pulse shaping," Opt. Lett. **26,** 557–559 (2001).
14. C.-C. Chang, H. P. Sardesai, and A. M. Weiner, "Dispersion-free fiber transmission for femtosecond pulses using a dispersion-compensating fiber and a programmable pulse shaper," Opt. Lett. **23,** 283–285 (1998).
15. S. Shen and A. M. Weiner, "Complete dispersion compensation for 400-fs pulse transmission over 10-km fiber link using dispersion compensating fiber and spectral phase equalizer," IEEE Photon. Technol. Lett. **11,** 827–829 (1999).
16. Z. Jiang, S. D. Yang, D. E. Leaird, and A. M. Weiner, "Fully dispersion-compensated ~500 fs pulse transmission over 50 km single-mode fiber," Opt. Lett. **30,** 1449–1451 (2005).
17. C. D. Poole and J. Nagel, "Polarization effects in lightwave systems," in *Optical Fiber Telecommunications,* I. P. Kaminow and T. L. Koch, eds. (Academic, 1997), Vol. IIIA.
18. H. Kogelnik, R. M. Jopson, and L. E. Nelson, "Polarization-mode dispersion," in *Optical Fiber Telecommunications,* I. Kaminow and T. Li, eds. (Academic, 2002), Vol. IVB.
19. M. Akbulut, A. M. Weiner, and P. J. Miller, "Wideband all-order polarization mode dispersion compensation via pulse shaping," Opt. Lett. **30,** 2691–2693 (2005).
20. M. Akbulut, A. M. Weiner, and P. J. Miller, "Broadband all-order polarization mode dispersion compensation using liquid-crystal modulator arrays," J. Lightwave Technol. **24,** 251–261 (2006).
21. S. X. Wang and A. M. Weiner, "Fast wavelength-parallel polarimeter for broadband optical networks," Opt. Lett. **29,** 923–925 (2004).
22. R. L. Peterson, R. E. Ziemer, and D. E. Borth, *Introduction to Spread-Spectrum Communications* (Prentice-Hall, 1995).
23. J. Shah, "Optical code division multiple access," Opt. Photon. News **14**(4), 42–47 (2003).
24. J. A. Salehi, A. M. Weiner, and J. P. Heritage, "Coherent ultrashort light pulse code-division multiple access communication systems," J. Lightwave Technol. **8,** 478 (1990).
25. A. M. Weiner, Z. Jiang, and D. E. Leaird, "Spectrally phase coded O-CDMA," J. Opt. Netw. **6,** 728–755 (2007).
26. J. P. Heritage and A. M. Weiner, "Advances in spectral optical code-division multiple-access communications," IEEE J. Sel. Top. Quantum Electron. **13,** 1351–1369 (2007).

27. Z. Jiang, D. S. Seo, S. D. Yang, D. E. Leaird, R. V. Roussev, C. Langrock, A. M. Fejer, and A. M. Weiner, "Four-user, 2.5-Gb/s, spectrally coded OCDMA system demonstration using low-power nonlinear processing," J. Lightwave Technol. **23,** 143–158 (2005).
28. Z. Jiang, D. Seo, S. Yang, D. E. Leaird, R. V. Roussev, C. Langrock, M. M. Fejer, and A. M. Weiner, "Four-user 10-Gb/s spectrally phase-coded O-CDMA system operating at similar to 30 fJ/bit," IEEE Photon. Technol. Lett. **17,** 705–707 (2005).
29. J. D. McKinney, I.-S. Lin, and A. M. Weiner, "Ultrabroadband arbitrary electromagnetic waveform synthesis," Opt. Photon. News **17**(4), 24–29 (2006).
30. J. D. McKinney and A. M. Weiner, "Photonic synthesis of ultrabroadband arbitrary electromagnetic waveforms," in *Advances in Microwave Photonics,* C. H. Lee, ed. (CRC Press, 2006).
31. J. Chou, Y. Han, and B. Jalali, "Adaptive RF-photonic arbitrary waveform generator," IEEE Photon. Technol. Lett. **15,** 581–583 (2003).
32. I. S. Lin, J. D. McKinney, and A. M. Weiner, "Photonic synthesis of broadband microwave arbitrary waveforms applicable to ultra-wideband communication," IEEE Microwave Wireless Components Lett. **15,** 226–228 (2005).
33. J. D. McKinney and A. M. Weiner, "Compensation of the effects of antenna dispersion on UWB waveforms via optical pulse-shaping techniques," IEEE Trans. Microwave Theory Tech. **54,** 1681–1686 (2006).
34. D. M. Pozar, "Waveform optimizations for ultrawideband radio systems," IEEE Trans. Antennas Propag. **51,** 2335–2345 (2003).
35. J. D. McKinney, D. Peroulis, and A. M. Weiner, "Dispersion limitations of ultrawideband wireless links and their compensation via photonically-enabled arbitrary waveform generation," IEEE Trans. Microwave Theory Tech. (submitted).